ChemPubSoc Europe

DOI: 10.1002/slct.201900622

Chemistry SELECT Full Papers

Inorganic Chemistry

Heterodimetallic Ferrocenyl Dithiophosphonate Complexes of Nickel(II), Zinc(II) and Cadmium(II) as Sensitizers for TiO_2-Based Dye-Sensitized Solar Cells

Tomilola J. Ajayi,[a] Moses Ollengo,[a] Lukas le Roux,[b] Michael N. Pillay,[a] Richard J. Staples,[c] Shannon M. Biros,[d] Kasper Wenderich,[e] Bastian Mei,[e] and Werner E. van Zyl*[a]

The formation, characterization, and dye sensitized solar cell application of nickel(II), zinc(II) and cadmium(II) ferrocenyl dithiophosphonate complexes were investigated. The multidentate monoanionic ligand $[S_2PFc(OH)]^-$ (**L1**) was synthesized. The reaction between metal salt precursors and **L1** produced Ni(II) complexes of the type $[Ni\{S_2P(Fc)(OH)\}_2]$ (**1**) (molar ratio 1:2), and a tetranickel(II) complex of the type $[Ni_2\{S_2OP(Fc)\}_2]_2$ (**2**) (molar ratio (1:1). It also produced a Zn(II) complex $[Zn\{S_2P(Fc)(OH)\}_2]_2$ (**3**), and a Cd(II) complex $[Cd\{S_2P(Fc)(OH)\}_2]_2$ (**4**). Complexes **1–4** were characterized by ^1H and ^{31}P NMR, FTIR and elemental analysis, and complexes **1** and **2** were additionally analyzed by X-ray crystallography. The first examples of dye-sensitized solar cells (DSSCs) co-sensitized with ferrocenyl dithiophosphonate complexes **1–4** are reported. Co-sensitization with the ruthenium dye N719, produced the dye materials (**3**)-N719 ($\eta = 8.30\%$) and (**4**)-N719 ($\eta = 7.78\%$), and they were found to have a better overall conversion efficiency than the pure Ru N719 dye standard ($\eta = 7.14\%$) under the same experimental conditions. The DSSCs were characterized using UV/vis, cyclic voltammetry, electrochemical impedance spectroscopy (EIS), photovoltaic- (I–V curves), and performing incident photon-to-current efficiency (IPCE) measurements.

Introduction

The world's energy demand is expected to reach 30 TW by the year 2050 at the present population growth rate.[1] High fossil fuel consumption linked to global warming and environmental pollution should be phased out and replaced with sustainable energy alternatives and technologies.[2] Solar cell research is at the forefront at harvesting clean, cheap and renewable energy,[3] and efforts to capture sunlight and convert it into electricity at high efficiency and with readily available materials remain both a scientific opportunity and challenge.[4] Since Grätzel and O'Regan reported the first dye-sensitized solar cells (DSSCs),[5] the result has drawn attention due to the high photon-to-electricity conversion efficiency, ease of fabrication, and low production cost involved.[6–9] As a result, investigations into metal complexes for photovoltaic applications have seen an increase.[10–12] A major obstacle in refining the efficiency of photovoltaic energy conversion concerns the spectral incompatibility between the energy distribution of photons in the incident solar spectrum and the bandgap of a chosen semiconductor material.[13]

Co-sensitization is an effective approach to advance the device performance through a combination of two or more dyes sensitized by the same semiconductor film and thus extending the light harvesting spectrum.[11,13] With the aim of finding efficient sensitizers, many new commercial[14–17] and synthetic dyes[18–20] have been investigated for spectral sensitization of wide-bandgap semiconductor electrodes.

The light-harvesting properties of the homo- and heteroleptic complexes of ferrocenyl dithiocarbamates have been reported,[21] as well as ferrocenyl dithiocarbonates as possible systems to be implemented in DSSCs, including ferrocenyl quinoxaline derivatives.[22,23] Misra and co-workers reported ferrocenyl-substituted triphenylamine-based donor–acceptor dyes for use in dye-sensitized solar cells.[24] Interest in the ferrocene-based systems stems from its well established redox features, and easily modified structure. Ferrocenyl systems have a characteristic electronic absorption band at around 450 nm[25,26] and therefore possesses the potential to compensate for the N719 dye's weakly absorbing lower-wavelength region. The N719 dye is a derivatized dianionic [Ru(II)bis(isothiocyanato)bis(2,2′-bipyridyl)] type complex; it has been extensively studied, and considered the gold standard in high performance dyes, and was used in the present study.

[a] *Dr. T. J. Ajayi, Dr. M. Ollengo, Dr. M. N. Pillay, Prof. W. E. van Zyl*
School of Chemistry and Physics, University of Kwazulu-Natal, Westville Campus, Durban. 4000. South Africa
Tel.: +27 31 260 3188
Fax: +27 31 260 3091
E-mail: vanzylw@ukzn.ac.za

[b] *Dr. L. le Roux*
MSM, Energy and Processes, Council for Scientific and Industrial Research (CSIR), Pretoria. South Africa.

[c] *Dr. R. J. Staples*
Department of Chemistry, Michigan State University, East Lansing, MI 48824–1322, USA

[d] *Prof. S. M. Biros*
Department of Chemistry, Grand Valley State University, Allendale, MI 49401, USA

[e] *Dr. K. Wenderich, Prof. B. Mei*
Photocatalytic Synthesis Group, MESA+ Institute for Nanotechnology, Faculty of Science and Technology, University of Twente, 7500 AE Enschede, The Netherlands

Supporting information for this article is available on the WWW under https://doi.org/10.1002/slct.201900622

In our ongoing work on phosphor-1,1-dithiolate complexes generally[27a–f] and the dithiophosphonate class of complexes in particular[27g–j] we turned our attention for the first time to the viability of multimetallic ferrocenyl dithiophosphonate complexes as low cost, high efficiency co-sensitizers in DSSCs. We synthesized two new nickel(II) (**1**-**2**), one zinc(II) (**3**) and one cadmium(II) (**4**) complex bearing the FcLR ligand. Further motivation for the work was to establish whether better efficiency can potentially be achieved through improved adhesion to the oxophilic titania substrate with the -OH moiety of the $[S_2PFc(OH)]^-$ ligand whilst keeping the dithiolato portion bonded to a metal.

Results and Discussion

Synthesis

The synthesis of Ni(II) ferrocenyl dithiophosphonate complexes obtained with different Ni:L ratios is shown in Scheme 1. The ammonium salt of the ferrocenyl dithiophosphonate ligand was prepared by ammonia gas bubbled into dithiophosphonic acid formed from the reaction between water and ferrocenyl Lawesson's reagent (FcLR) in an equimolar ratio (2:1). FcLR undergoes a ring opening reaction allowing cleavage of the dimer and produced ammonium salt that was isolated as a bright yellow powder. Previously, various groups of alcohols had been used for FcLR, including methanol, ethanol, and isopropanol[28] and ring opening by ammonia hydrate have been reported.[29] A number of ligands through a combination of S/N/O heterocyclic atoms have been used in the nucleophilic ring opening reaction of the FcLR reagent.[30–33] The metal complexation chemistry of FcLR is generally scarce, with only a few complexes known,[28] whilst reported metal complexes with the new hydroxy ferrocenyl dithiophosphonate ligand **L1** is heretofore unknown.

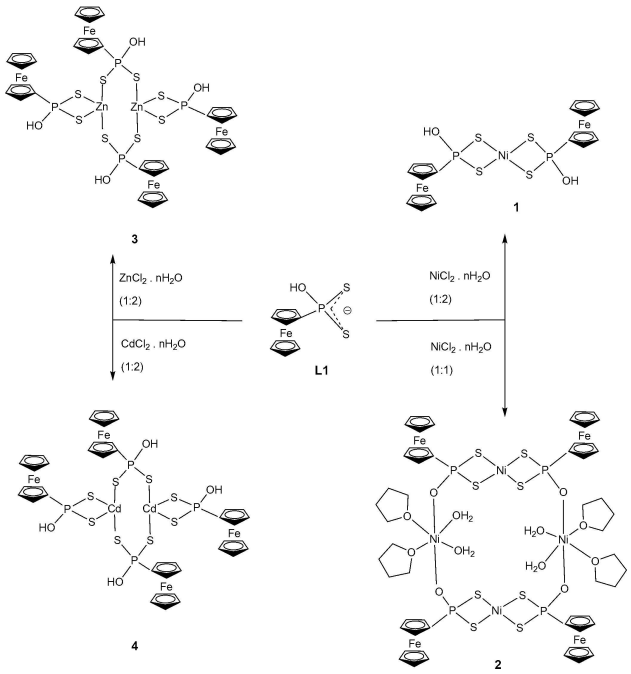

Scheme 1. Synthesis of ferrocenyl dithiophosphonate nickel(II), zinc(II) and cadmium(II) complexes prepared in different M:L mole ratios

We report the synthesis of two nickel(II), one cadmium(II) and one zinc(II) complexes (**1**-**4**). The crystal structures of **1** and **2** were determined by X-ray crystallographic analysis. The structures of **3** and **4** were not determined by X-ray analysis. Their related molecular structure (as depicted in Scheme 1) has been established by previous reports where the P–O-R moiety was used instead of our P–O-H (for the purpose of potentially more efficient binding to titania surface). We therefore are confident about the nature of the structure proposed for **3** and **4** formed in a (1:2) metal: ligand ratio, and additionally supported by elemental analysis results.[28] Complexes **3** and **4** are isomorphous and consists of dinuclear Zn(II) and Cd(II) units surrounded by four **L1** ligands, two binding in a chelating mode, and two in a bridging mode.

Characterization

The ligand **L1** is soluble in polar solvents such as water, methanol, and ethanol. The ^{31}P NMR spectrum of the ligand displayed a sharp singlet at 58.8 ppm, which was a substantial upfield shift as a result of the P-OH moiety. The IR spectrum shows strong bands at 1175, 1024, 584 and 488 cm^{-1} for **L1**, these stretches we attribute to ν(P–O–C), ν(P–O–C), $\nu(PS)_{asym}$ and $\nu(PS)_{sym}$ stretching vibrations, respectively. To obtain information on the possible structure of the binding of the dyes onto the TiO_2 surface of the DSSC electrode, the Fourier transform infrared (FTIR) spectra of complexes **1–4** and of the complexes adsorbed onto the TiO_2 surface were measured. The FTIR spectra of complexes **1–4** showed a common absorption band at 3031 cm^{-1}, which is assigned to the hydroxyl groups of the complexes. However, the FTIR spectra of complexes **1–4** sensitized TiO_2 films displayed characteristic bands at 2767 cm^{-1} assigned to the P-O stretching vibrations, coordinated to surface atoms of titania, with subsequent disappearance of the band at 3031 cm^{-1}. This observation suggests deprotonation of the P–O-H group, with binding and electronic coupling of the dyes onto the TiO_2 surface.

The metal complexes **1–4** were isolated in varying yields (46–87%) as either brown Ni(II), or yellow Cd(II) and Zn(II) powders. Complexes **1**, **3** and **4** are air-stable and partially soluble in dichloromethane, chloroform, and THF and soluble in polar solvents such as ethanol, methanol, and water. These types of complexes are typically not soluble in polar solvents and we propose the introduction of hydroxyl groups aided solubility. Complex **2** is not air stable for a prolonged period and neither accurate elemental analysis nor ^1H NMR could not be recorded. A satisfactory X-ray structure for **2** could be obtained, however, presumably because the grown single crystal was kept cold (100 K) and in an inert atmosphere during data recording, but upon warming up the solvent molecules (THF and water) coordinated to the Ni center starts slowly leaks

out of the crystal. The ^{31}P NMR spectra of all the complexes display sharp singlet peaks. The IR spectra of compounds **1–4** were very similar to that of the free ligand, indicating that they were virtually unchanged by complexation.

X-ray structures

The reaction between the Ni(II) precursor and **L1** in molar ratio 1:2 produced complex **1** (Figure 1), while molar ratio 1:1

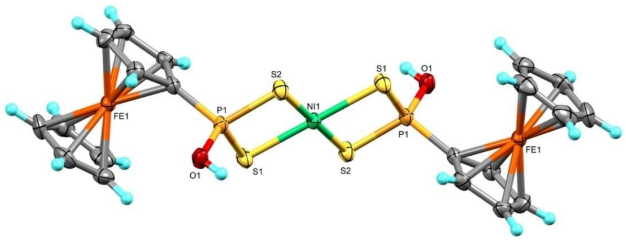

Figure 1. ORTEP molecular structure of Ni(II) complex prepared in ratio 1:2.

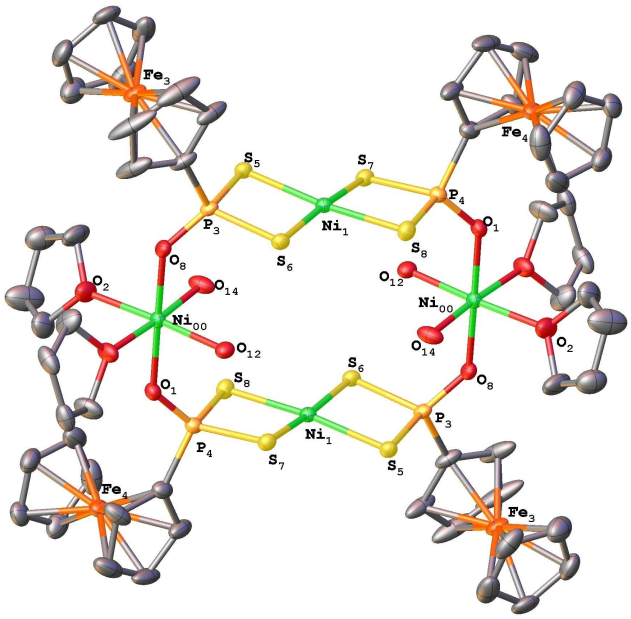

Figure 2. ORTEP molecular structure of Ni(II) complex prepared in M:L ratio of 1:1. Atom labeling in accord with one of the two molecules in the unit cell. Hydrogen atoms are omitted for clarity.

produced complex **2** (Figure 2), as confirmed by X-ray crystal structures. Both structures showed a square planar geometry around the Ni centre with symmetric MS_2P rings. The structure of **1** displays a typical *trans* configuration where the ferrocenyl groups are arranged diagonally opposite the central metal center. Select bond lengths and angles are summarized in Table 1. The Ni(1)-S(1) bond length is slightly longer (2.23 Å) than the Ni(1)-S(2) bond length (2.21 Å) suggesting the latter has slight double bond character and the complex is not an ideal isobidentate structure.

Table 1. Select bond lengths (Å) and angles (°) for complex **1**

Ni(1)-S(1)	2.2338(8)	S(2)-Ni(1)-S(1)	88.33(3)
Ni(1)-S(2)	2.2172(8)	S(2)#1-Ni(1)-S(1)	91.67(3)
S(1)-P(1)	2.0066(11)	S(2)-Ni(1)-S(2)#1	180.0
S(2)-P(1)	2.0109(11)	P(1)-S(1)-Ni(1)	85.11(4)
P(1)-O(1)	1.569(2)	P(1)-S(2)-Ni(1)	85.45(3)
P(1)-C(1)	1.768(3)	S(1)-P(1)-S(2)	101.05(5)
S(1)#1-Ni(1)-S(1)	180.0	O(1)-P(1)-S(1)	115.46(10)
S(2)-Ni(1)-S(1)#1	91.67(3)	O(1)-P(1)-S(2)	112.55(9)

In contrast, complex **2** shows a rare *cis* configuration where a ferrocenyl group of each nickel complex unit are arranged on the same side of the metal coordination plane. The *cis* arrangement was presumably enforced by the formation of the large metallocycle. Interestingly, in the 16-member cycle, not a single heteroatom is carbon. The only other *cis* configurations we are aware of was found in Ni(II) and Pd(II) complexes, respectively, and both were stabilized by an extensive hydrogen bonding network.[34]

The molecular structure of **2** is a tetranickel(II) tetraferrocenyl square-planar complex containing both 4- and 6-coordination around the two different Ni(II) centers. The octahedral arrangement for each Ni(II) center is made up of the P–O portion of the ligand (O donor atom) in the axial position, whilst the equatorial positions are occupied by 2 water molecules (positioned 'inside' the macrocycle, presumably due to less steric crowding), and 2 THF molecules on the 'outside' of the macrocycle. There are two formula units in the unit cell (Z = 2). Selected bond lengths and angles for one of the molecules in the unit cell of complex **2** are summarized in Table 2. The Ni–O(1) and Ni–O(12) (phosphonate) bond lengths

Table 2. Select bond lengths (Å) and angles (°) for complex **2**

Ni(00)-O(1)	2.0387(16)	O(8)-Ni(00)-O(1)	178.79(7)
Ni(00)-O(2)	2.0660(18)	O(12)-Ni(00)-O(1)	89.40(7)
Ni(00)-O(8)	2.0341(16)	O(12)-Ni(00)-O(2)	174.72(8)
Ni(00)-O(12)	2.0493(17)	S(6)-Ni(1)-S(5)	87.92(2)
Ni(1)-S(5)	2.2207(6)	S(7)-Ni(1)-S(6)	173.44(2)
Ni(1)-S(6)	2.2195(6)	S(5)-P(3)-O(8)#2	115.53(7)
Ni(1)-S(7)	2.2128(6)	S(6)-P(3)-S(5)	97.71(3)
Ni(1)-S(8)	2.0392(8)		

are as expected quite similar at 2.039 and 2.034 Å which is shorter (presumably due to the formal anionic charge on the O atom) than the Ni–O(12) (water) 2.049 Å bond length, which in turn is shorter than the Ni–O(2) (THF) bond length at 2.066 Å. For the sulfur-Ni(II) center, all the Ni–S bond lengths are virtually the same. For example, the Ni(1)-S(5) and Ni(1)-S(6) bond lengths are both essentially 2.22 Å. Around the (sulfur)-Ni(II), (oxygen)-Ni(II) and P-atom centers, the respective geo-

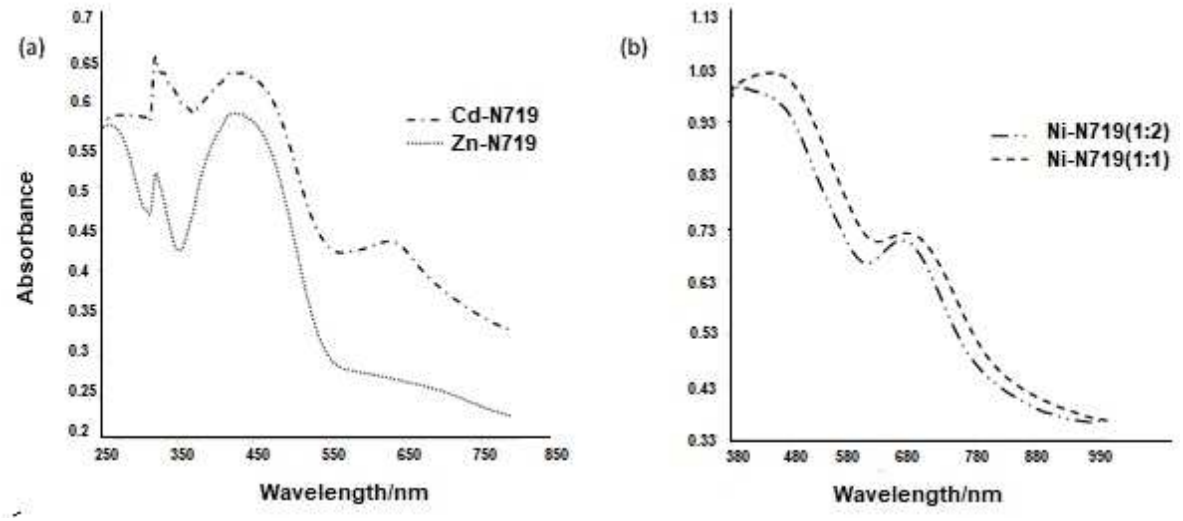

Figure 3. Electronic absorption spectra of the co-sensitizers, complexes **1–4**.

metries can all be described as slightly distorted square planar, -octahedral, and –tetrahedral.

Optical Properties of the Co-Sensitizers

The optical properties were determined by UV/Vis absorption and photoluminescence (PL) experiments carried out on complexes **1–4** both in solution and solid state, Figure 3a and b. The Ni(II) complexes **1** and **2** showed absorptions in the 380 to 480 nm region and low energy absorption bands around 680 nm which tails to 980 nm. Both complexes **3** and **4** displayed three absorptions near 260, 325 and 450 nm, in the same range to what has been reported for Cd(II) pyridyl/ ferrocene dithiocarbamate complexes.[21b]

For complexes with ligands having low-lying π^* orbitals, transitions can occur at low energy, as seemed to be the case in **1** and **2**. The low energy region could be attributed to the availability of low-lying empty 3d orbitals that allow an S atom to act as an acceptor and the preference of sulfur for metal centers that are not highly oxidizing.[35] The π^* orbitals of the Cp ligand are located at higher energies and is considered a CT donor. Low-energy LMCT transitions occur if Cp coordinates to oxidizing metals.[36,37] However, for Cp complexes containing acceptor ligands, LMCT absorptions may be observed and cause luminescence.[38,39] The photoluminescence of group 12 metals are of general importance due to the absence of d-d bands interfering in the visible region. In this work, however, only the Cd(II) complex **4** showed luminescence in the solid state, Figure 4.

This could be attributed to aggregation-induced emission over the region ranging from 400–500 nm observed only in the solid state. The closed-shell Zn(II) and Cd(II) d^{10} complexes **3** and **4** are not readily prone to redox and do not significantly influence ligand absorption bands making MLCT generally unlikely, but there is a possibility of outer sphere charge transfer (OSCT) excitations which are related to MLCT.[38] Low-

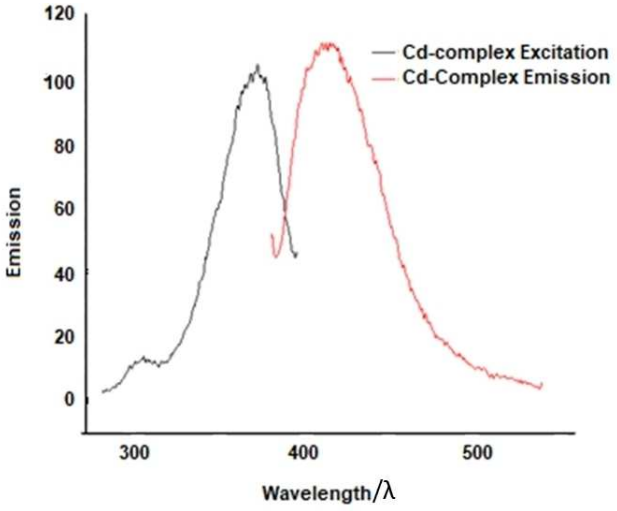

Figure 4. Solid state photoluminescent spectra of the co-sensitizer Cd(II) complex **4**.

lying MLCT and ligand-centered (π–π^*) excited states of Cp-based complexes are relatively long-lived to participate in electron transfer processes.

In complexes **1–4**, the highest occupied molecular orbitals (HOMO) are in the Cp σ-bond while the lowest unoccupied molecular orbitals (LUMO) are antibonding with regard to the P–S-M bond. Hence, the longest wavelength absorption was assigned to a $d\sigma^*$ transition terminating at the bridging sulfur atom.[39]

Complexes **1–4** have broad absorption spectra with intense LLCT, LMCT and MLCT bands overlapping the solar spectrum, affording suitable photoelectrochemical properties for application in solar cells. The hydroxy groups provide an avenue for strong adsorption to a TiO_2 surface and the necessary electronic coupling between the charge-transfer excited states

Table 3. Details of X-ray data collection and refinement.

Compound	1	2
Formula	$C_{20}H_{20}Fe_2NiO_2P_2S_4 \cdot 2(C_4H_8O)$	$C_{56}H_{76}Fe_4Ni_4O_{12}P_4S_8$
$D_{calc.}$/ g cm^{-3}	1.633	1.537
μ/mm^{-1}	1.847	2.041
Formula Weight	797.16	1779.80
Colour	yellow	brown
Shape	plate	chunk
Max Size/mm	0.198	0.420
Mid-Size/mm	0.180	0.220
Min Size/mm	0.043	0.140
T/K	173(2)	100(2)
Crystal System	monoclinic	triclinic
Space Group	$P2_1/c$	$P-1$
a/Å	15.0135(17)	14.1756(9)
b/Å	8.0033(9)	15.9831(11)
c/Å	14.9346(17)	18.8891(12)
∝/°	90	84.280(2)
β/°	115.3950(10)	70.822(2)
γ/°	90	71.957(2)
V/Å^3	1621.1(3)	3843.4(4)
Z	2	2
Measured Refl.	16921	60457
Independent Refl.	2955	18710
Completeness to theta	25.242	25.242
R_{int}	0.0550	0.0246
Parameters	191	825
Restraints	0	18
Largest Peak/eÅ^{-3}	0.69	1.17
Deepest Hole/eÅ^{-3}	-0.31	-0.63
GoF on F^2	1.063	1.057
wR_2 (all data)	0.0863	0.0689
wR_2	0.0807	0.0651
R_1 (all data)	0.0446	0.0284
R_1	0.0345	0.0363
F(000)	820.0	1833.0

(CTES) of the sensitizers and the wave function of the semiconductor conduction band. Consequently, dye excitation with visible light is likely to produce very fast electron transfer through the appended groups to the semiconductor.[40] The energy band gaps for the complexes was estimated from their UV/Vis spectra by use of Tauc plots, Table 4.

Electrochemical Properties of Co-Sensitizers

In DSSCs, energy matching is of significance and cyclic voltammetry (CV) was employed in this study to determine the HOMO levels and the LUMO levels of the synthesized complexes. Experimental data and electrochemical properties of Ni, Zn, and Cd complexes are reported in Table 4. An illustration of the relative energy levels of the HOMO and LUMO energy gaps for different complexes are shown in Scheme 2.

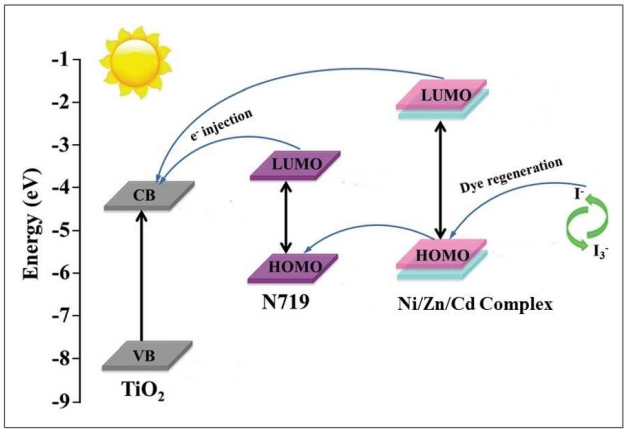

Scheme 2. A schematic energy diagram of HOMO and LUMO levels for the co-sensitizers compared to the energy levels calculated for TiO_2, after ref. 11.

$$E_{HOMO}\ (eV) = -e\ (E_{ox}/Vvs.SCE^{d} + 4.4) \quad (1)$$

$$E_{LUMO}\ (eV) = E_{HOMO}\ (eV) + E_{0-0}{}^{ci}\ (eV) \quad (2)$$

From Table 4 the HOMO values for Ni(II), Zn(II), and Cd(II) complexes were calculated to be −4.75, −4.93, −4.79 and −4.83 eV, while the LUMO levels were calculated to be −2.90, −2.93, −2.54 and −2.68 eV using equations 1 and 2.[11,41] The LUMO level of a sensitizer should be above the conduction band (CB) of the TiO_2 semiconductor (−4.40 eV vs. vacuum) for efficient electron injection, while the HOMO energy level should stay below the energy level of the I^-/I_3^- redox couple (−4.85 eV vs. vacuum) for regeneration.[42] Our experimental data confirmed the case for the prepared complexes, and their LUMO are also higher than free N719 dye. Therefore, co-sensitizing the state-of-the-art N719 dye with complexes **1–4** will result in a greater synergistic effect, which should improve the electron injection efficiency from the LUMO of the dye to the conduction band of TiO_2.

Table 4. Experimental data for the spectral and electrochemical properties of **1–4**.

	$\lambda^a{}_{abs}$(nm)	ε^b(M^{-1}cm^{-1})	$E_{0-0}{}^c$ (eV)	E_{ox}/V vs SCE^d	$E_{HOMO}{}^e$(eV)	$E_{LUMO}{}^e$(eV)
1	462	102050	1.85	0.35	-4.75	-2.90
2	406	99620	2.00	0.53	-4.93	-2.93
3	441	58140	2.25	0.39	-4.79	-2.54
4	439	63220	2.15	0.43	-4.83	-2.68

[a] Absorption recorded in a DMSO solution (10^{-5} M) at room temperature. [b] The molar absorptivity calculated from absorption spectra. [c] Optical band gap. [d] The first oxidation potentials of complexes obtained from CV measurement. [e] The values of E_{HOMO} and E_{LUMO} were calculated with the following formula:[33]

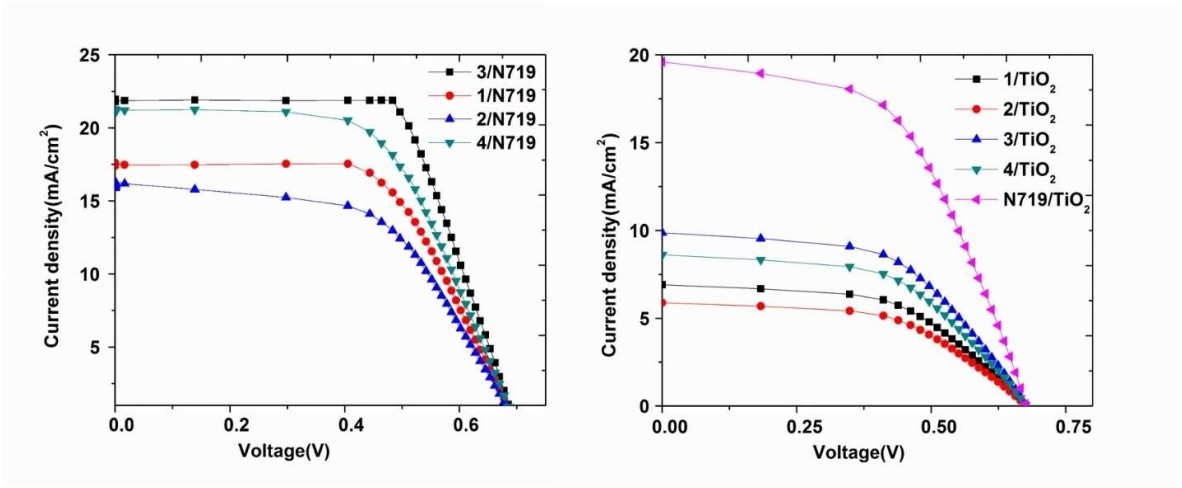

Figure 5. *J–V* curves for DSSCs based on N719- co-sensitized with different ferrocenyl dithiophosphonate complexes and N719-sensitized photoelectrodes under irradiation.

Photovoltaic Properties

The Ni(II), Zn(II), and Cd(II) complexes were employed as co-sensitizers and co-adsorbents to fabricate complex-N719 photoanodes. The current–voltage characteristics of the DSSC devices based on ordinary N719 dye, complexes **1–4** and the co-sensitized Ni–N719, Zn–N719, and Cd–N719 photoanodes are shown in Figure 5 and the data are summarized in Table 5.

Table 5. *J* - V performance of DSSCs based on different photoelectrodes.

Electrodes	J_{SC}[mA cm^{-2}]	V_{OC}[V]	FF	η (%)
N719	19.60	0.667	0.55	7.19
1	6.91	0.651	0.54	2.43
2	5.88	0.651	0.53	2.03
3	9.87	0.659	0.55	3.58
4	8.61	0.658	0.55	3.12
1/N719	17.44	0.680	0.56	6.63
2/N719	16.70	0.685	0.56	6.40
3/N719	21.52	0.665	0.58	8.30
4/N719	20.49	0.665	0.57	7.78

For comparison, the result obtained with the use of N719 dye under the same experimental conditions is included. The cell parameters derived from these curves are also summarized. The complexes **1–4** sensitized device exhibited a η value of 2.43%, 2.03%, 3.58% and 3.12%, respectively. The lower conversion efficiency, η value for devices sensitized by the individual complex co-sensitizers is attributed to their narrow adsorption band. It was observed that cells containing the N719 dye co-sensitized with complexes **3** and **4** showed improved performance above the efficiency of conventional N719 dye. The overall conversion efficiency achieved with this complex **3**-N719 dye (η = 8.30%) and complex **4**-N719 dye (η = 7.78%) compared favorably to that of N719 dye (η = 7.14%) under the same experimental conditions. The high efficiencies of the co-sensitized N719 dye with different ferrocenyl dithiophosphonate complexes (Ni(II), Zn(II) & Cd(II)) may be linked to the electronic properties of ferrocenyl contained in these complexes. The influence of the number of ferrocenyl groups on performance of N719 dye co-sensitized with nickel (II) complex was also investigated. Complex **1** contained two ferrocenyl and **2** has four ferrocenyl groups formed from two different nickel to ligand ratios.

Electrochemical impedance spectra analysis

In an effort to study the dynamics of the electron-transport properties and charge recombination processes in the interfacial regions of the solid/liquid layers involving these complexes, electrochemical impedance spectra (EIS) were obtained. The Nyquist spectra were analyzed by fitting varied electrical equivalent circuit elements to obtain the 'best-fit' circuit model that represents the investigated system. Four different fits were obtained, shown in Figure 6. All complexes presented a semi-circle associated with the electron/charge transfer at the TiO_2/dye/electrolyte interface[43] for different circuit models. The equivalent circuits represent three different contributions which result in the total resistance of the system. The ohmic resistance of the electrolytes in **4**- and **3**-N719 cells, R1 is due to charge transfer, while R2 are attributed to dissociative adsorption on the electrode surface and R3 in **3**-N719 interfacial charge diffusion. R1 and R2 have constant phase elements (CPE) in parallel to simulate the distribution of relaxation time in the real system.[44,45]

The diameter of semicircles decreases in the order **3**-N719 > **4**-N719 indicating a decrease in recombination resistance at the TiO_2/ dye/electrolyte interface. This indicates retardation of charge recombination between injected electrons and I^{3-} ions in the electrolyte, and as a result, a rise in open circuit voltage was observed (from 0.665 to 0.685 V). A similar observation was made by Yadav et al.[46] who concluded that co-sensitization of

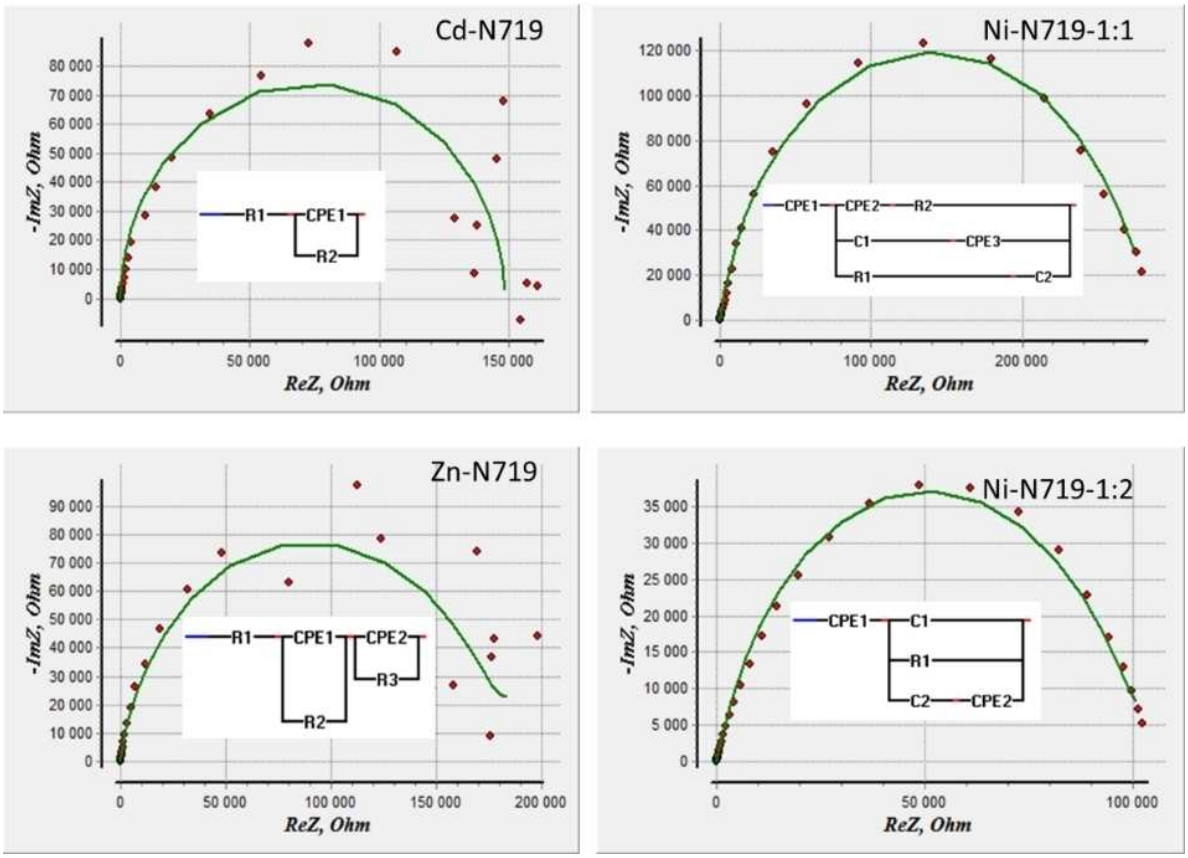

Figure 6. Electrochemical impedance measurement fitted data for complexes **1**–**4**.

the N719 dye with metal dithiocarbamates complexes favours DSSCs performance. Our results showed a higher efficiency of 8.30 and 7.78% for **3**- and **4**-N719, respectively. The nickel(II) complexes in the metal to ferrocenyl ligand ratio of 1:1 and 1:2 gave different circuit fits. Notably, the **1**-N719 (1:2) complex indicated much higher impedance characteristics compared to **2**-N719 (1:1). The **2**-N719 (1:1) cell was expected to show higher performance efficiency than observed due to multi ferrocenyl groups present on the co-sensitized complex. Counterintuitively, there was more resistance, and thus the impedance increased, which may be largely due to the presence of two more nickel centers and additional coordinated THF and water groups, the latter is known to increase the resistance.[47] The complexes indicated a higher number of capacitive elements in their corresponding equivalent circuits, which indicate a delay between the current and the potential, attributed to less efficient intramolecular charge transfer. The high electrical double layer resistance in **1**-N719 indicate poor electron transport.[48] The consequence is the observed low efficiency 6.28 and 6.81% for **1**-N719 and **2**-N719, respectively. However, their low optical band gap, 1.8 and 2.00 eV indicate the charge accumulation and thus higher open circuit voltage of 0.685 and 0.680 V compared to the N719. This indicates the percolation of charge is a less efficient process.[49] It can be argued that the system is charge conserving and that the two systems can be good at charge storing.

To further determine electron transport time (τ_d) which is a measure of the rate of an electron injected to the collecting electrode, the electron lifetime was estimated from the peak frequency of the Bode phase plots. The τ_d values were calculated using the expression adopted from Gao, et al.[50] shown in Eq. (3)

$$\tau_d = \frac{1}{2\pi f_{peak}} \quad (3)$$

The values were 1.98 and 2.18 ms for **4**-N719 and **3**-N719, respectively and 1.98 and 1.04 ms for **2**-N719 and **1**-N719, respectively. A shorter time is associated with a higher photocurrent. The estimated τ_d value for N719 was 2.65 ms which implied that the back-charge recombination was suppressed in all investigated systems. The observed difference in the performance of these systems is presumably due to their structural differences.

Incident photon-to-current efficiency (IPCE) measurements

The incident photon to current efficiencies (% IPCE) spectrum of the Ni, Zn and Cd N719 co-sensitizers are shown in Figure 7. The current was measured as a function of the wavelength of the monochromatic light in the 400 to 700 nm range. Compared with the other optical results described above, the

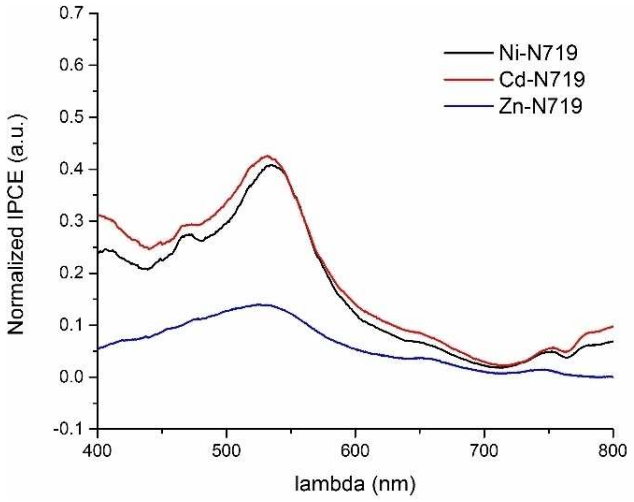

Figure 7. Photocurrent action spectra (IPCE (a.u.) vs. λ) of co-sensitized Ni–N719, Zn–N719, and Cd–N719 complexes.

IPCE measurements were substandard. For the pure complexes **1**, **3**, and **4** representing the metals Ni, Zn and Cd, we could not find a statistically significant spectrum in the 400–460 nm region. Upon co-sensitization with N719, the same complexes did show an improvement as expected, but the increase was not remarkable in the region 400–700 nm, compared to other reports for similar metals.[21] Hence, the IPCE result can only be interpreted as a trend observed. The cadmium complex showed the best IPCE response, followed by nickel and zinc.

Conclusions

The first reaction of ferrocenyl Lawesson's Reagent with water is described for the formation of a dithiophosphonate ligand leading to complexes with multimetallic and multiferrocenyl assemblies. Our investigations revealed that the new synthesized ferrocenyl dithiophosphonate complexes are capable to work as efficient co-sensitizers with Ru N719 dye in DSSC. The photovoltaic performance of co-sensitizers are in the order Zn/N719 > Cd/719 > Ni/719 > Ni_4/719. The highest current density was achieved for the group 12 metals at 21.89 and 21.80 mA/cm^2 for Zn(II) and Cd(II), respectively, exceeding the gold standard of free Ru719 at 17.44 mA/cm^2. The complexes are capable of improving *J*sc as well as *V*oc, and each of the fabricated cells shows better performance than the DSSC fabricated by using solely the N719 dye. The IPCE results require more fine-tuning to compete with current state-of-the-art systems. Taken as a whole, the study opens new avenues to be explored for the use of ferrocene-based dithiophosphonate ligand complexes and their application as co-sensitizers in solar cell research.

Supporting Information Summary

Supporting information contains: experimental section with relevant references, and Nyquist plots recorded for all materials. CCDC 1535619 and 1534976 and crystallographic data and tables for complexes **1** and **2**.

Acknowledgements

The CCD based X-ray diffractometer at Michigan State University were upgraded and/or replaced by departmental funds. We thank the Eskom TESP grant (#P677) for financial support of this work.

Conflict of Interest

The authors declare no conflict of interest.

Keywords: Crystal structures · DSSC · Electrical impedance spectroscopy · Ferrocenyl-dithiophosphonates · Group 12 elements

[1] N. S. Lewis, D. G. Nocera, *Proc. Natl. Acad. Sci.* **2006**, *103*, 15729–15735.
[2] C. J. Campbell, *Pop. Environ.* **2002**, *24*, 193–207.
[3] R. F. Service, *Science* **2014**, *344*, 458.
[4] a) J. Liu, Y. Liu, N. Y. Liu, Y. Z. Han, X. Zhang, H. Huang, Y. Lifshitz, S.-T. Lee, J. Zhong, Z. H. Kang, *Science* **2015**, *347*, 970–974; b) M. Z. Yu, W. D. McCulloch, D. R. Beauchamp, Z. J. Huang, X. D. Ren, Y. Y. Wu, *J. Am. Chem. Soc.* **2015**, *137*, 8332–8335; c) H. Wang, J. T. Yang, X. Li, H. Z. Zhang, J. H. Li, L. Guo, *Small* **2012**, *8*, 2802—2806.
[5] B. O'Regan, M. Grätzel, *Nature* **1991**, *353*, 737–740.
[6] M. Chandrasekharam, G. Rajkumar, C. Srinivasa Rao, T. Suresh, P. Y. Reddy, Y. Soujanya, *J. Chem. Sci.* **2011**, *123*, 555–565.
[7] S. G. Chen, S. Chappel, Y. Diamant, A. Zaban, *Chem. Mater.* **2001**, *13*, 4629–4634.
[8] M. Grätzel, *Nature* **2001**, *414*, 338–344.
[9] a) M. Grätzel, *J. Photochem. Photobiol. Photochem. Rev.* **2003**, *4*, 145–153. b) M. Grätzel, *Acc. Chem. Res.* **2009**, *42*, 1788.
[10] X. Huang, S. Han, W. Huang and X. Liu, *Chem. Soc. Rev.* **2013**, *42*, 173–201.
[11] S. Gao, R. Q. Fan, X. M. Wang, L. S. Qiang, L. G. Wei, P. Wang, Y. L. Yang, Y. L. Wang, *Dalton Trans.* **2015**, *44*, 18187–18195.
[12] Y.-J. Wang, W.-L. Chen, L. Chen, X.-T. Zheng, S.-S. Xu, E.-B. Wang, *Inorg. Chem. Front.* **2017**, *4*, 559–565
[13] T. Stergiopoulos, P. Falaras, *Adv. Energy Mater.* **2012**, *2*, 616–627.
[14] A. M. Bagher, M. M. A. Vahid, M. Mohsen, *Am. J. Optics Photon.* **2015**, *3*, 94–113.
[15] K. Hara, T. Horiguchi, T. Kinoshita, K. Sayama, H. Sugihara, H. Arakawa, *Sol. Energy Mater. Sol. Cells* **2000**, *64*, 115–134.
[16] A. Kumar, R. Chauhan, K. C. Molloy, G. Kociok-Köhn, L. Bahadur, N. Singh, *Chem. Eur. J.* **2010**, *16*, 4307–4314.
[17] A. Kay, R. Humphry-Baker, M. Grätzel, *J. Phys. Chem.* **1994**, *98*, 952–959.
[18] a) F. J. Malzner, M. Willgert, E. C. Constable, C. E. Housecroft, *J. Mater. Chem A* **2017**, *5*, 13717–13729; b) L. Bahadur, L. Roy, *Semicond. Sci. Tech.* **1995**, *10*, 358.
[19] M. K. Nazeeruddin, M. Grätzel, *J. Photochem.Photobiol. Chem.* **2001**, *145*, 79–86.
[20] C. G. Garcia, A. K. Nakano, C. J. Kleverlaan, N. Y. Murakami Iha, *J. Photochem.Photobiol. Chem.* **2002**, *151*, 165–170.
[21] a) K. K. Manar, Neetu, Anamika, P. Srivastava, M. G. B. Drew, N. Singh, *ChemistrySelect* **2017**, *2*, 8301–8311; b) Neetu, K. K. Manar, P. Srivastava, N. Singh, *Solar Energy* **2018**, *176*, 312–319.
[22] R. Chauhan, S. Auvinen, A. S. Aditya, M. Trivedi, R. Prasad, M. Alatalo, D. P. Amalnerkar, A. Kumar, *Solar Energy* **2014**, *108*, 560–569.
[23] R. Chauhan, M. Shahid, M. Trivedi, D. P. Amalnerkar, A. Kumar, *Eur. J. Inorg. Chem.*, **2015**, *2015*, 3700–3707.
[24] R. Misra, R. Maragani, K. R. Patel, G. D. Sharma, *RSC Adv.* **2014**, *4*, 34904–34911.
[25] H. B. Gray, Y. S. Sohn, N. Hendrickson, *J. Am. Chem. Soc.* **1971**, *93*, 3603–3612.

[26] A. T. Armstrong, F. Smith, E. Elder, S. P. McGlynn, *J. Chem. Phys.* **1967**, *46*, 4321–4328.
[27] a) R. S. Dhayal, W. E. van Zyl, C. W. Liu, *Acc. Chem. Res.* **2016**, *49*, 86–95; b) R. S. Dhayal, J.-H. Liao, S. Kahlal, X. Wang, Y.-C. Liu, M.-H. Chiang, W. E. van Zyl, J.-Y. Saillard, C. W. Liu, *Chem.– Eur. J.* **2015**, *21*, 8369–8374; c) R. S. Dhayal, W. E. van Zyl, C. W. Liu, *Dalton Trans.* **2019**, *48*, 3531–3538; d) R. S. Dhayal, H.-P. Chen, J.-H. Liao, W. E. van Zyl, C. W. Liu, *ChemistrySelect* **2018**, *3*, 3603–3610; e) J.-H. Liao, H.-W. Chang, Y.-J. Li, C.-S. Fang, B. Sarkar, W. E. van Zyl, C. W. Liu, *Dalton Trans.* **2014**, *43*, 12380–12389; f) Y.-C. Lee, Y.-R. Lin, B.-Y. Liou, J.-H. Liao, N. K. Gusarova, B. A. Trofimov, W. E. van Zyl, C. W. Liu, *Dalton Trans.* **2014**, *43*, 663–670; g) W. E. van Zyl, J. D. Woollins, *Coord. Chem. Rev.* **2013**, *257*, 718–731; h) M. N. Pillay, B. Omondi, R. J. Staples, W. E. van Zyl *CrystEngComm* **2013**, *15*, 4417–4421; i) W. E. van Zyl *Comments Inorg. Chem.* **2010**, *31*, 13–45; j) T. J. Ajayi, M. N. Pillay, W. E. van Zyl, *Phos. Sulf. Silicon & Relat. Elem.* **2017**, *192*, 1205–1211.
[28] a) I. P. Gray, A. M. Z. Slawin, J. Derek Woollins *Z. Anorg. Allg. Chem.* **2004**, *630*, 1851–1857; b) I. P. Gray, H. L. Milton, A. M. Z. Slawin, J. D. Woollins, *Dalton Trans* **2003**, 3450; c) M. N. Pillay, H. van der Walt, R. J. Staples, W. E. van Zyl *J. Organomet. Chem.* **2015**, *794*, 33–39; d) M. Karakus, P. Lönnecke, D. Yakhvarovc, E. Hey-Hawkins, *Z. Anorg. Allg. Chem.* **2004**, *630*, 1444–1450; e) S.-L. Liu, X.-Y. Wang, T. Duan, W.-H. Leung, Q.-F. Zhang, *J. Mol. Struct.* **2010**, *964*, 78–81
[29] X.-Y. Wang, Y. Li, Q. Ma, Q.-F. Zhang, *Organometallics* **2010**, *29*, 2752–2760.
[30] W. Shi, M. Shafaei-Fallah, C. E. Anson, A. Rothenberger, *Dalton Trans.* **2005**, 3909–3912.
[31] W. Shi, R. Kelting, M. Shafaei-Fallah, A. Rothenberger, *J. Organomet. Chem.* **2007**, *692*, 2678–2682.
[32] E. G. Sağlam, S. Erden, Ö. Tutsak, D. E. Bayraktepe, Z. Y. Durmuş, H. Dal, A. Ebinç, *Phos. Sulf. Silicon & Relat. Elem.* **2017**, *192*, 322–329.
[33] G. K. Çılgı, M. Karakuş, M. Ak, *Synth. Metals* **2013**, *180*, 25–31.
[34] a) V. G. Albano, M. C. Aragoni, M. Arca, C. Castellari, F. Demartin, F. A. Devillanova, F. Isaia, V. Lippolis, L. Loddo, G. Verani, *Chem. Comm.* **2002**, 1170–1171; b) M. C. Aragoni, M. Arca, F. Demartin, F. A. Devillanova, F. Isaia, V. Lippolis, G. Verani *Inorg. Chim. Acta* **2005**, *358*, 213–216.
[35] A. Vogler, H. Kunkely, *Coord. Chem. Rev.* **2000**, *208*, 321–329.
[36] A. Vogler, H. Kunkely, *Coord. Chem. Rev.* **2004**, *248*, 273–278.
[37] Y. Yamaguchi, W. Ding, C. T. Sanderson, M. L. Borden, M. J. Morgan, C. Kutal, *Coord. Chem. Rev.* **2007**, *251*, 515–524.
[38] A. Vogler, H. Kunkely, *Coord. Chem. Rev.* **2001**, *211*, 223–233.
[39] H. Kunkely, V. Arnd, *J. Organomet. Chem.* **1998**, *568*, 291–293 >.
[40] C. G. Garcia, J. F. de Lima, N. Y. Murakami Iha, *Coord. Chem. Rev.* **2000**, *196*, 219–247.
[41] C. M. Cardona, W. Li, A. E. Kaifer, D. Stockdale, G. C. Bazan, *Adv. Materials* **2011**, *23*, 2367–2371.
[42] K. R. J. Thomas, Y.-C. Hsu, J. T. Lin, K.-M. Lee, K.-C. Ho, C.-H. Lai, Y.-M. Cheng, P.-T. Chou, *Chem. Mater.* **2008**, *20*, 1830–1840.
[43] R. Pinedo, I. Ruiz de Larramendi, N. Ortiz-Vitoriano, I. Gil de Muro, T. Rojo, *J. Power Sources* **2012**, *201*, 332–339.
[44] J. Sacanell, M. G. Bellino, D. G. Lamas and A. G. Leyva, *Physica B: Cond. Matter* **2007**, *398*, 341–343.
[45] X. Chen, S. Wang, Y. L. Yang, L. Smith, N. J. Wu, B. I. Kim, S. S. Perry, A. J. Jacobson, A. Ignatiev, *Solid State Ionics* **2002**, *146*, 405–413.
[46] R. Yadav, M. Trivedi, G. Kociok-Köhn, R. Chauhan, A. Kumar, S. W. Gosavi, *Eur. J. Inorg. Chem.* **2016**, *2016*, 1013–1021.
[47] N. Perini, A. R. Prado, C. M. S. Sad, E. V. R. Castro, M. B. J. G. Freitas, *Fuel* **2012**, *91*, 224–228.
[48] H. Maeda, R. Sakamoto, H. Nishihara, *J. Phys. Chem. Lett.* **2015**, *6*, 3821–3826.
[49] K. Kalyanasundaram, M. Gratzel, *Coord. Chem. Rev.* **1998**, *77*, 347–414.
[50] S. Gao, R. Q. Fan, X. M. Wang, L. S. Qiang, L. G. Wei, P. Wang, Y. L. Yang, Y. L. Wang, *Dalton Trans.* **2015**, *44*, 18187–18195.

Submitted: February 18, 2019
Accepted: June 17, 2019